

1

2

THÈSE DE DOCTORAT DE

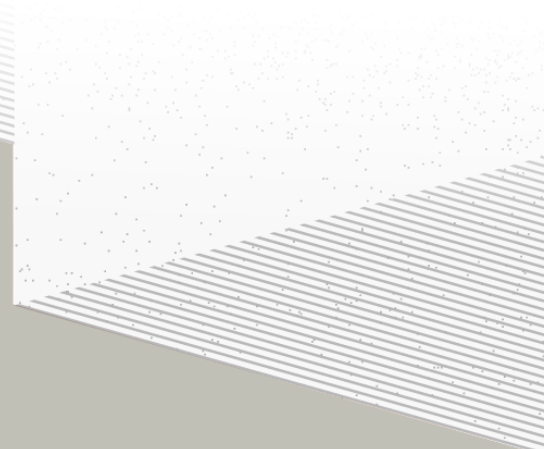
L'UNIVERSITÉ DE NANTES

ÉCOLE DOCTORALE N°596
Matière, Molécules, Matériaux
Spécialité : *Physique des particules*

Par

Léonard Imbert

**Precision measurement of solar neutrino oscillation parameters
with the JUNO small PMTs system and test of the unitarity of the
PMNS matrix**



Thèse présentée et soutenue à Nantes, le Too soon and too early at the same time
Unité de recherche : Laboratoire SUBATECH, UMR 6457

Rapporteurs avant soutenance :

Someone	Very high position, Somewhere
Someone else	Another high position, Somewhere else

Composition du Jury :

Président :	Jacques Chirac	French president, France
Examinateurs :	Yoda	Master, Dagobha
Dir. de thèse :	Frédéric Yermia	Professeur, Université de Nantes
Co-dir. de thèse :	Benoit Viaud	Chargé de recherche, CNRS

Invité(s) :

Victor Lebrin Docteur, CNRS/SUBATECH

³ List of Abbreviations

ACU	Automatic Calibration Unit
CD	Central Detector
CLS	Cable Loop System
GT	Guiding Tube
IBD	Inverse Beta Decay
IO	Inverse Ordering
JUNO	Jiangmen Underground Neutrino Observatory
LPMT	Large PMT
LS	Liquid Scintillator
NMO	Neutrino Mass Ordering
NO	Normal Ordering
PE	Photo Electron
PMT	Photo-Multipliers Tubes
ROV	Remotely Operated under-LS Vehicle
SPMT	Small PMT
TTS	Time Transit Spread
TT	Top Tracker
WCD	Water Cherenkov Detector

4 Contents

5	Contents	1
6	Remerciements	3
7	Introduction	5
8	1 Neutrino physics	7
9	1.1 Standard model	7
10	1.1.1 Limits of the standard model	7
11	1.2 Historic of the neutrino	7
12	1.3 Oscillation	7
13	1.3.1 Phenomologies	7
14	1.4 Open questions	7
15	2 The JUNO experiment	9
16	2.1 Neutrinos physics in JUNO	9
17	2.1.1 $\bar{\nu}_e$ flux coming from nuclear power plants	9
18	2.1.2 Reactor neutrino oscillation for NMO and precise measurements	10
19	2.1.3 Other physics	12
20	2.2 The JUNO detector	13
21	2.2.1 Principle of detection	14
22	2.2.2 Central Detector (CD)	14
23	2.2.3 Veto detector	18
24	2.3 Calibration strategy	19
25	2.3.1 Energy scale calibration	19
26	2.3.2 Calibration system	20
27	2.4 Software	21
28	2.5 State of the art of the IBD reconstruction in JUNO	21
29	2.5.1 Interaction vertex reconstruction	21
30	2.5.2 Energy reconstruction	22
31	2.5.3 Particle identification	22
32	2.5.4 Machine learning for reconstruction	22
33	2.6 JUNO sensitivity to NMO and precise measurements	22
34	2.6.1 Fitting procedure	22

35	3 Machine learning and Artificial Neural Network	23
36	3.1 History of the Machine learning	23
37	3.2 Boosted Decision Tree (BDT)	23
38	3.3 Artificial Neural Network (NN)	23
39	3.3.1 Fully Connected Deep Neural Network (FCDNN)	23
40	3.3.2 Convolutional Neural Network (CNN)	23
41	3.3.3 Graph Neural Network (GNN)	23
42	3.3.4 Adversarial Neural Network (ANN)	23
43	4 Image recognition for IBD reconstruction with the SPMT system	25
44	5 Graph representation of JUNO for IBD reconstruction with the LPMT system	27
45	6 Reliability of machine learning methods	29
46	7 Discrimination of e+/e- events in JUNO	31
47	8 Conclusion	33
48	Bibliography	35

⁴⁹ Remerciements

⁵⁰ Introduction

⁵¹ **Chapter 1**

⁵² **Neutrino physics**

⁵³

The neutrino, or ν for the close friends, a fascinating and invisible particle. Some will say that dark matter also have those property but at least we are pretty confident that neutrinos exists.

⁵⁴ **1.1 Standard model**

⁵⁵ **1.1.1 Limits of the standard model**

⁵⁶ **1.2 Historic of the neutrino**

⁵⁷ **First theories**

⁵⁸ **Discovery**

⁵⁹ **Milestones and anomalies**

⁶⁰ **1.3 Oscillation**

⁶¹ **1.3.1 Phenomologies**

⁶² **1.4 Open questions**

Decrire le m
Regarder th
Kochebina
Limite du r
Interessant,
les neutrino
CP ? Pb des

⁶³ **Chapter 2**

⁶⁴ **The JUNO experiment**

⁶⁵ “*Ave Juno, rosae rosam, et spiritus rex*”. It means nothing but I found it in tone.

⁶⁶ The first idea of a medium baseline (~ 60 km) experiment, was explored in 2008 where it was
⁶⁷ demonstrated that the Neutrino Mass Ordering (NMO) could be determined by a medium base-
⁶⁸ line experiment if $\sin^2(2\theta_{13}) > 0.005$ without requirements on accurate information of the reactor
⁶⁹ antineutrino spectra and the value of Δm_{32}^2 [1]. From this idea is born the Jiangmen Underground
⁷⁰ Neutrino Observatory (JUNO) experiment.

⁷¹ JUNO is a neutrino detection experiment under construction located in China. Its main objectives
⁷² are the determination of the mass ordering at the $3\text{-}4\sigma$ level in 6 years of data taking and the mea-
⁷³ surement at the per-mil precision of the oscillation parameters Δm_{21}^2 , $\sin^2 \theta_{12}$, Δm_{32}^2 and, with less
⁷⁴ precision, $\sin^2 \theta_{13}$ [2].

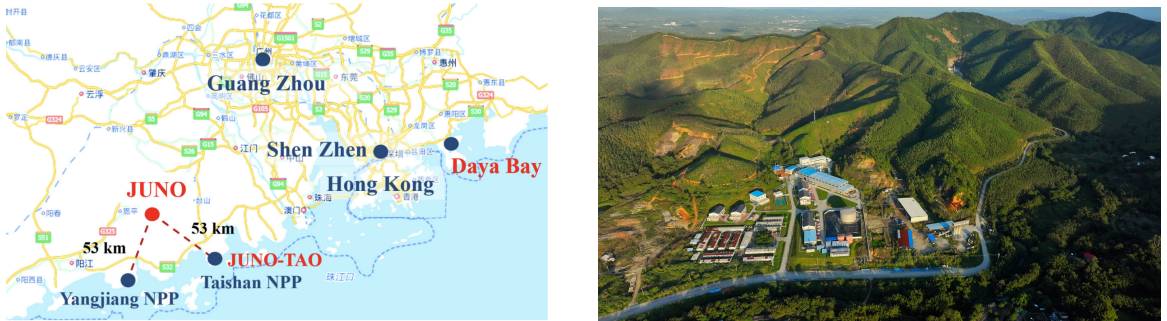


FIGURE 2.1 – On the left: Location of the JUNO experiment and its reactor sources in southern china. On the right: external view of the experimental site

⁷⁵ For this JUNO will measure the electronic anti-neutrinos ($\bar{\nu}_e$) flux coming from the nuclear reac-
⁷⁶ tors of Taishan, Yangjiang, for a total power of 26.6 GW_{th} , and the Daya Bay power plant to a lesser
⁷⁷ extent. Details about the power plants and there expected flux of $\bar{\nu}_e$ can be found in the table 2.1. The
⁷⁸ distance of 53 km has been specifically chosen to maximize the disappearance probability of the $\bar{\nu}_e$.

⁷⁹ **2.1 Neutrinos physics in JUNO**

⁸⁰ **2.1.1 $\bar{\nu}_e$ flux coming from nuclear power plants**

⁸¹ To get such high measurements precision, it is necessary to have a very good understanding of the
⁸² source characteristics. For its main studies, JUNO will measure the energy of neutrinos coming from
⁸³ core of nuclear power plants of Taishan and Yangjiang, located at 53 km of the detector to maximise
⁸⁴ the disappearance probability of the $\bar{\nu}_e$.

Reactor	Power (GW _{th})	Baseline (km)	IBD Rate (day ⁻¹)	Relative Flux (%)
Taishan	9.2	52.71	15.1	32.1
Core 1	4.6	52.77	7.5	16.0
Core 2	4.6	52.64	7.6	16.1
Yangjiang	17.4	52.46	29.0	61.5
Core 1	2.9	52.74	4.8	10.1
Core 2	2.9	52.82	4.7	10.1
Core 3	2.9	52.41	4.8	10.3
Core 4	2.9	52.49	4.8	10.2
Core 5	2.9	52.11	4.9	10.4
Core 6	2.9	52.19	4.9	10.4
Daya Bay	17.4	215	3.0	6.4

TABLE 2.1 – Characteristics of the nuclear power plants observed by JUNO. The IBD rate are estimated from the baselines, the reactors full thermal power, selection efficiency and the current knowledge of the oscillation parameters

The $\bar{\nu}_e$ coming from reactors are emitted from β -decay of unstable fission fragments. The Taishan and Yangjiang reactors are pressurised water reactor (PWR), the same type as Daya Bay. In those type of reactor more than 99.7 % and $\bar{\nu}_e$ are produced by the fissions of four fuel isotopes ^{235}U , ^{238}U , ^{239}Pu and ^{241}Pu . The neutrino flux per fission of each isotope is determined by the inversion of the measured β spectra of fission product [3–7] or by calculation using the nuclear databases [8, 9]. The neutrino flux coming from a reactor at a time t can be predicted using

$$\phi(E_\nu, t)_r = \frac{W_{th}(t)}{\sum_i f_i(t) e_i} \sum_i f_i(t) S_i(E_\nu) \quad (2.1)$$

where $W_{th}(t)$ is the thermal power of the reactor, $f_i(t)$ is the fraction fission of the i th isotope, e_i its thermal energy released in each fission and $S_i(e_\nu)$ the neutrino flux per fission for this isotope. Using this method, the flux uncertainty is expected to be of an order of 2-3 % [10].

In addition to those prediction, a satellite experiment named TAO[11] will be setup the reactor core Taishan -1 to measure with an energy resolution of 2% at 1 MeV the neutrino flux coming from the core to identify unknown fine structure and give more insight on the $\bar{\nu}_e$ flux coming from this reactor.

One the current open issue about the reactor neutrino flux is the so-called neutrino anomaly, an unexpected surplus of neutrino emission in the spectra around 5 MeV [12]. Multiples scientists are trying to explain this surplus by advanced recalculation of the nuclei model during beta decay [13, 14] but no consensus on this issue has been reached yet.

2.1.2 Reactor neutrino oscillation for NMO and precise measurements

Previous works [1, 15] shows that oscillation parameters and the NMO can be observed by looking at the $\bar{\nu}_e$ disappearance spectrum coming from medium baseline nuclear reactor. This disappearance probability can be expressed as [2] :

$$P(\bar{\nu}_e \rightarrow \bar{\nu}_e) = 1 - \sin^2 2\theta_{12} c_{13}^4 \sin^2 \frac{\Delta m_{21}^2 L}{4E} - \sin^2 2\theta_{13} \left[c_{12}^2 \sin^2 \frac{\Delta m_{31}^2 L}{4E} + s_{12}^2 \sin^2 \frac{\Delta m_{32}^2 L}{4E} \right]$$

Where $s_{ij} = \sin \theta_{ij}$, $c_{ij} = \cos \theta_{ij}$, E is the $\bar{\nu}_e$ energy and L is the baseline. We can see the sensitivity to the NMO in the dependency to Δm_{32}^2 and Δm_{31}^2 causing a phase shift of the spectrum as we can see in the figure 2.2. By carefully fitting this spectrum, one can extract the NMO and the oscillation parameters. The fit is reviewed in more details in the section 2.6.1

To reach the desired sensitivity, JUNO must meet multiple requirements but most notably:

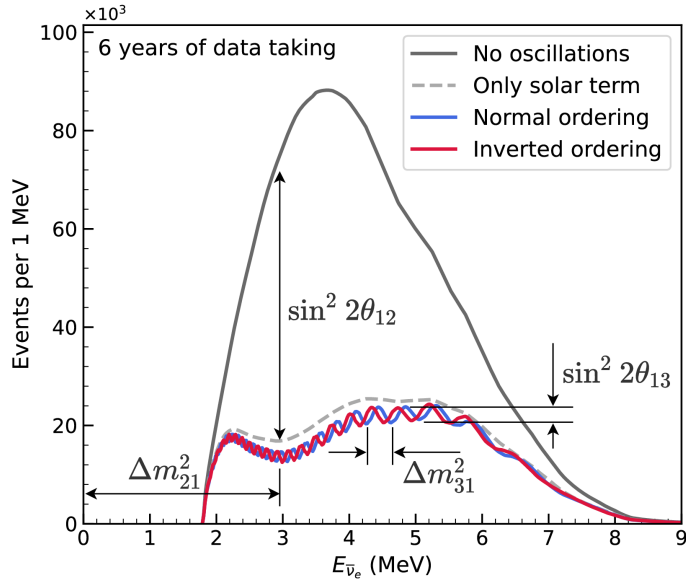


FIGURE 2.2 – Expected number of neutrinos event per MeV in JUNO after 6 years of data taking. The black curve shows the flux if there was no oscillation. The light gray curve shows the oscillation if only the solar terms are taken in account (θ_{12} , Δm_{21}^2). The blue and red curve shows the spectrum in the case of, respectively, NO and IO. The dependency of the oscillation to the different parameters are schematized by the double sided arrows. We can see the NMO sensitivity by looking at the fine phase shift between the red and the blue curve.

- ¹⁰⁸ 1. An energy resolution of $3\%/\sqrt{E(\text{MeV})}$ to be able to distinguish the fine structure of the fast
- ¹⁰⁹ oscillation.
- ¹¹⁰ 2. An energy precision of 1% in order to not err on the location of the oscillation pattern.
- ¹¹¹ 3. A baseline of 53 ± 0.5 km to maximise the $\bar{\nu}_e$ oscillation probability.
- ¹¹² 4. At least $\approx 100,000$ events to limit the spectrum distortion due to statistical uncertainties.

¹¹³ Identification of the mass ordering

¹¹⁴ To identify the mass ordering, we fit the neutrino energy spectrum under the two hypothesis of
¹¹⁵ NO and IO. Those two fits give us two χ^2 , respectively χ^2_{NO} and χ^2_{IO} . By computing the difference
¹¹⁶ $\Delta\chi^2 = \chi^2_{NO} - \chi^2_{IO}$ we can determine the most probable mass ordering: NO if $\Delta\chi^2 > 0$ and IO
¹¹⁷ if $\Delta\chi^2 < 0$. Current studies show that the expected sensitivity to the mass ordering would be of
¹¹⁸ 3.4σ after 6 years of data taking in nominal setup[2]. More detailed explanations about the fitting
¹¹⁹ procedure can be found in the section 2.6.1.

¹²⁰ Precise measurement of the oscillation parameters

¹²¹ The oscillation parameters θ_{12} , θ_{13} , Δm_{21}^2 , Δm_{31}^2 are free parameters in the fit of the oscillation
¹²² spectrum. The precision on those parameters have been estimated and are shown in figure 2.3. We
¹²³ see that for θ_{12} , Δm_{21}^2 , Δm_{31}^2 , precision at 6 years is better than the reference precision by an order of
¹²⁴ magnitude [10]

125 **2.1.3 Other physics**

126 While the design of JUNO is tailored to measure $\bar{\nu}_e$ coming from nuclear reactor, JUNO will be
 127 able to detect neutrinos coming from other sources thus allowing for a wide range of physics studies
 128 as detailed in the table 2.2 and in the following sub-section.

Research	Expected signal	Energy region	Major backgrounds
Reactor antineutrino	60 IBDs/day	0–12 MeV	Radioactivity, cosmic muon
Supernova burst	5000 IBDs at 10 kpc	0–80 MeV	Negligible
DSNB (w/o PSD)	2300 elastic scattering		
Solar neutrino	2–4 IBDs/year	10–40 MeV	Atmospheric ν
Atmospheric neutrino	hundreds per year for ${}^8\text{B}$	0–16 MeV	Radioactivity
Geoneutrino	hundreds per year	0.1–100 GeV	Negligible
	≈ 400 per year	0–3 MeV	Reactor ν

TABLE 2.2 – Detectable neutrino signal in JUNO and the expected signal rates and major background sources

129 **Geoneutrinos**

130 Geoneutrinos designate the antineutrinos coming from the decay of long-lived radioactive elements
 131 inside the Earth. The 1.8 MeV threshold necessary for the IBD makes it possible to measure
 132 geoneutrinos from ${}^{238}\text{U}$ and ${}^{232}\text{Th}$ decay chains. The studies of geoneutrinos can help refine the Earth
 133 crust models but is also necessary to characterise their signal, as they are a background to the mass
 134 ordering and oscillations parameters studies.

135 **Atmospheric neutrinos**

136 Atmospheric neutrinos are neutrinos originating from the decay of π and K particles that are
 137 produced in extensive air showers initiated by the interactions of cosmic rays with the Earth atmosphere.
 138 Earth is mostly transparent to neutrinos below the PeV energy, thus JUNO will be able to see
 139 neutrinos coming from all directions. Their baseline range is large (15km \sim 13000km), they can have
 140 energy between 0.1 GeV and 10 TeV and will contain all neutrino and antineutrinos flavour. Their
 141 studies is complementary to the reactor antineutrinos and can bring constraint on the MO [2].

142 **Beyond standard model neutrinos interactions**

143 JUNO will also be able to probe for beyond standard model neutrinos interactions. After that
 144 the main physics topics have been accomplished, JUNO could be upgraded to probe for neutrinoless
 145 beta decay ($0\nu\beta\beta$). The detection of such event would give critical informations about the nature
 146 of neutrinos, is it a majorana or a dirac particle. JUNO will also be able to probe for neutrinos that
 147 would come for the decay or annihilation of Dark Matter inside the sun and neutrinos from putative

	Central Value	PDG2020	100 days	6 years	20 years
Δm_{31}^2 ($\times 10^{-3}$ eV 2)	2.5283	± 0.034 (1.3%)	± 0.021 (0.8%)	± 0.0047 (0.2%)	± 0.0029 (0.1%)
Δm_{21}^2 ($\times 10^{-5}$ eV 2)	7.53	± 0.18 (2.4%)	± 0.074 (1.0%)	± 0.024 (0.3%)	± 0.017 (0.2%)
$\sin^2 \theta_{12}$	0.307	± 0.013 (4.2%)	± 0.0058 (1.9%)	± 0.0016 (0.5%)	± 0.0010 (0.3%)
$\sin^2 \theta_{13}$	0.0218	± 0.0007 (3.2%)	± 0.010 (47.9%)	± 0.0026 (12.1%)	± 0.0016 (7.3%)

FIGURE 2.3 – A summary of precision levels fir the oscillation parameters. The reference value (PDG 2020 [16]) is compared with 100 days, 6 years and 20 years of JUNO data taking.

¹⁴⁸ primordial black hole. Through the unitary test of the mixing matrix, JUNO will be able to search
¹⁴⁹ for light sterile neutrinos. Thanks to JUNO sensitivity, multiple other exotic can be performed on
¹⁵⁰ neutrino related beyond standard model interactions.

¹⁵¹ Supernovae burst neutrinos

¹⁵² Neutrinos are crucial component during all stages of stellar collapse and explosion. Detection
¹⁵³ of neutrinos coming for core collapse supernovae will provide us important informations on the
¹⁵⁴ mechanisms at play in those events. Thanks to its 20 kt LS, JUNO has excellent capabilities to detect
¹⁵⁵ all flavour of the $\mathcal{O}(10 \text{ MeV})$ postshock neutrinos, and using neutrinos of the $\mathcal{O}(1 \text{ MeV})$ will give
¹⁵⁶ informations about the pre-supernovae neutrinos. All those informations will allow to disentangle
¹⁵⁷ between the multiple hydro-dynamic models that are currently used to describe the different stage
¹⁵⁸ of the core-collapse.

¹⁵⁹ Diffuse supernovae neutrinos background

¹⁶⁰ Core-collapse supernovae in our galaxy are rare events, but they frequently occur throughout the
¹⁶¹ visible Universe sending burst of neutrinos in direction of the Earth. All those events contributes to
¹⁶² a low background flux of low-energy neutrinos called the Diffuse Supernovae Neutrino Background
¹⁶³ (DSNB). Its flux and spectrum contains informations about the red-shift dependent supernovae rate,
¹⁶⁴ the average SN neutrino energy and the fraction of black-hole formation in core-collapse supernovae.
¹⁶⁵ Depending of the DSNB model, we can expect 2-4 IBD events per year in the energy range above the
¹⁶⁶ reactor $\bar{\nu}_e$ signal, which is competitive with the current Super-Kamiokande+Gadolinium phase [17].

¹⁶⁷ Background in the neutrinos reactor spectrum

¹⁶⁸ Considering the close reactor neutrinos flux as the main signal, the signals that are considered as
¹⁶⁹ background are:

- ¹⁷⁰ — The geoneutrinos producing background in the $0.511 \sim 2.7 \text{ MeV}$ region.
- ¹⁷¹ — The neutrinos coming from the other nuclear reactors around Earth.

¹⁷² In addition to all those physics signal, non-neutrinos signal that would mimic an IBD will also be
¹⁷³ present. It is composed of:

- ¹⁷⁴ — The signal coming from radioactive decay (α, γ, β) from natural radioactive isotopes in the
¹⁷⁵ material of the detector.
- ¹⁷⁶ — Cosmogenic event such as fast neutrons and activated isotopes induced by muons passing
¹⁷⁷ through the detector, most notably the spallation on ^{12}C .

¹⁷⁸ All those events represent a non-negligable part of the spectrum as shown in figure 2.4.

¹⁷⁹ 2.2 The JUNO detector

¹⁸⁰ The JUNO detector is a scintillator detector buried 693.35 under the ground (1800 meters water
¹⁸¹ equivalent). It consist of Central Detector (CD), a water cherenkov detector and a Top Tracker as
¹⁸² scheme in figure 2.5. The CD is an acrylic vessel containing the 20 ktons of LS. It is supported by a
¹⁸³ stainless steel structure and is immersed in a water that serve as shielding from external radiation
¹⁸⁴ and a cherenkov detector for the background. The top of the experiment is partially covered with the
¹⁸⁵ TT, a plastic scintillator detector which is use to detect the atmospheric muons background acting as
¹⁸⁶ veto detector. The top of the experiment also host the LS purification system, a water purification
¹⁸⁷ system, a ventilation system to get rid of the potential radon in the air. The CD is observed by two
¹⁸⁸ system of photo-multipliers tubes (PMT). They are attached to the steel structure and their electronic
¹⁸⁹ readout is partially submersed near them. A third observation system of PMT is also installed on the
¹⁹⁰ structure but are facing outward of the CD, instrumenting the water to be cherenkov detector. The
¹⁹¹ CD and the cherenkov detector are optically separated by Tyvek sheet. A chimney for LS filling and
¹⁹² purification and for calibration operations connects the CD to the experimental hall from the top.

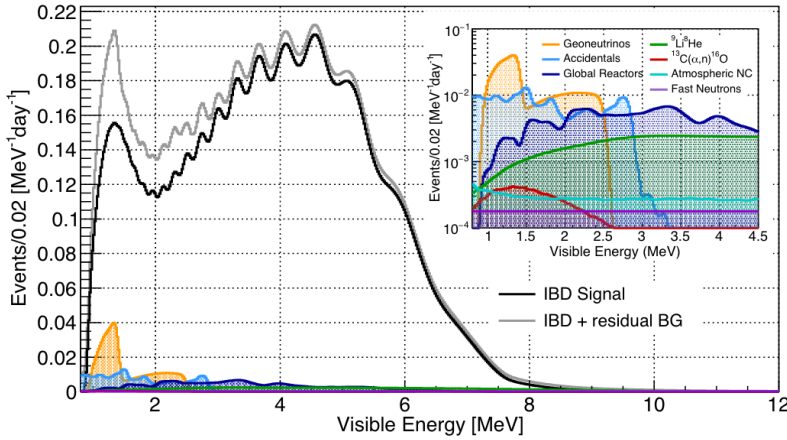


FIGURE 2.4 – Expected visible energy spectrum measured with the LPMT system with (grey) and without (black) backgrounds. The background amount for about 7% of the IBD candidate and are mostly localized below 3 MeV [10]

193 2.2.1 Principle of detection

The CD will detect the neutrino and measure their energy mainly via an Inverse Beta Decay (IBD) interaction with the proton of the LS:

$$\bar{\nu}_e + p \rightarrow n + e^+$$

194 Simple kinematics calculation shows that the $\bar{\nu}_e$ must have an energy of $(m_n + m_e - m_p) \approx 1.806$ MeV
195 [18] where m_λ is the mass of the λ particle. This threshold make the experiment blind to very low
196 energy neutrinos. The residual energy $E_\nu - 1.806$ MeV is be distributed as kinetic energy between
197 the positron and the neutron. The energy of the emitted positron E_e is given by [18]

$$E_e = \frac{(E_\nu - \delta)(1 + \epsilon_\nu) + \epsilon_\nu \cos \theta \sqrt{(E_\nu - \delta)^2 + \kappa m_e^2}}{\kappa} \quad (2.2)$$

198 where $\kappa = (1 + \epsilon_\nu)^2 - \epsilon_\nu^2 \cos^2 \theta \approx 1$, $\epsilon_\nu = \frac{E_\nu}{m_p} \ll 1$ and $\delta = \frac{m_n^2 - m_p^2 - m_e^2}{2m_p} \ll 1$. We can see from this
199 equation that the positron energy is strongly correlated to the neutrino energy.

200 Once the positron and the neutron will propagate in the detection medium, the liquid scintillator
201 (LS), loosing their kinetic energy by exciting with the LS. Once stopped, the positron will annihilate
202 with an electron from the medium producing two 511 KeV gamma. Those gamma will themselves
203 interact with the LS, exciting it before being absorbed by photoelectrical effect. The neutron will be
204 captured by an hydrogen, emitting a 2.2 MeV gamma in the process. This gamma will also deposit
205 its energy before being absorbed by the LS.

206 More details about the LS can be found in section 2.2.2.

207 The scintillation photons have an UV frequency and will be captured by PMTs observing the
208 CD. The analogue signal, then digitized by the electronic is the signal of our experiment. The signal
209 produced by the positron is subsequently called the prompt signal, and the signal coming from the
210 neutron the delayed signal. This naming convention come from the fact that the positron will deposit
211 its energy rather quickly (few ns) where the neutron will take a bit more time ($\sim 236 \mu\text{s}$).

212 2.2.2 Central Detector (CD)

213 The central detector, composed of 20 ktons of Liquid Scintillator (LS) is the main part of JUNO.
214 The LS is contained in a spherical acrylic vessel of inner diameter of 35.4 m and a thickness of 120
215 mm. The CD and its structural support are submerged in a cylindrical water pool of 43.5m diameter

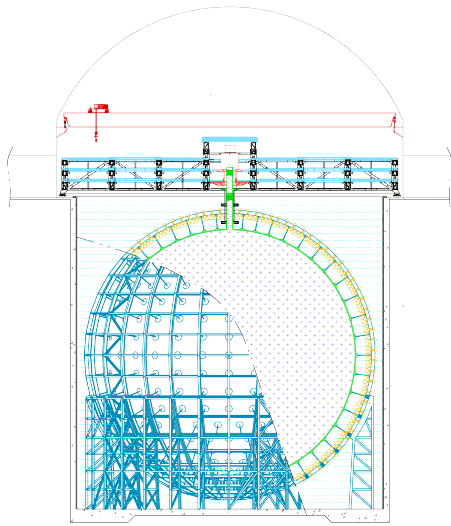


FIGURE 2.5 – Schematics view of the JUNO detector.

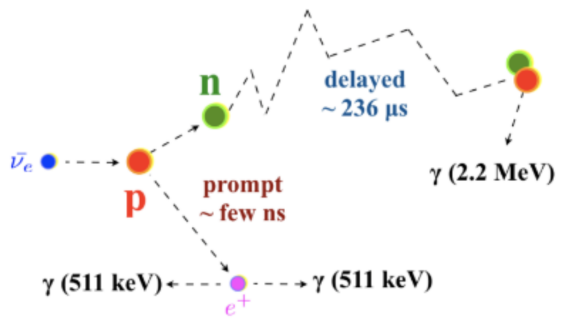


FIGURE 2.6 – Schematics of an IBD interaction in the central detector of JUNO

and 44 m height. We're confident that the water pool provide sufficient buffer protection in every direction against the rock radioactivity.

Acrylic vessel

The acrylic vessel is a spherical vessel of 35.4 m inner diameter. It is assembled from 265 acrylic panels, thermo bonded together. The acrylic recipes has been carefully tuned with extensive R&D to ensure it does not include plasticizer and anti-UV material that would stop the scintillation photons. Those panels require to be pure of radioactive materials to not cause background. Current setup where the acrylic panels are molded in cleanrooms of class 10000, let us reach a uranium and thorium contamination of <0.5 ppt. The molding and thermoforming processes is optimized to increase the assemblage transparency in water to >96%. The acrylic vessel is supported by a stainless steel structure via supporting node (fig 2.7). The struccture and the node are designed to be resilient to natrual event such as earthquake and support many times the effective load of the acrylic vessel.

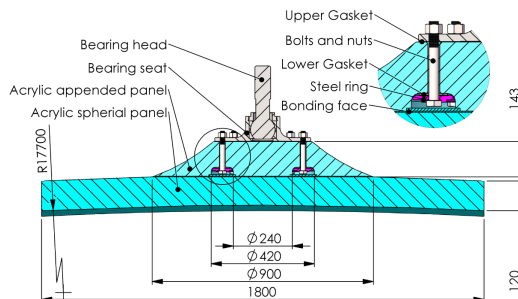


FIGURE 2.7 – Schematics of the supporting node for the acrylic vessel

228 Liquid scintillator

229 The Liquid Scintillator (LS) has a similar recipe as the one used in Daya Bay [19] but without
230 gadolinium doping. It is made of three components, necessary to shift the wavelength of emitted
231 photon to prevent reabsorption by the LS:

- 232 1. The detection medium is the *linear alkylbenzene* (LAB), selected because of its excellent trans-
233 parency, high flash point, low chemical reactivity and good light yield. Representing $\sim 98\%$ of
234 the LS, it is the main component with which ionizing particles and gamma interact. Charged
235 particles will collide with its electronic cloud, transferring energy to the molecule, gamma will
236 interact via compton effect with the electronic cloud before finally be absorbed via photoelec-
237 tric effect.
- 238 2. The second component of the LS is the *2,5-diphenyloxazole* (PPO). A fraction of the excitation
239 energy of the LAB is transferred to the PPO, mainly via non radiative process [20]. The
240 PPO molecules de-excites in the same way, transferring their energy to the bis-MSB. The PPO
241 makes for 1.5% of the LS.
- 242 3. The last component is the *p-bis(o-methylstyryl)-benzene* (bis-MSB). Once excited by the PPO, it
243 will emit photon with an average wavelength of ~ 430 nm (full spectrum in figure 2.8) that
244 can be detected by our photo-multipliers systems. It amount for $\sim 0.5\%$ of the LS.

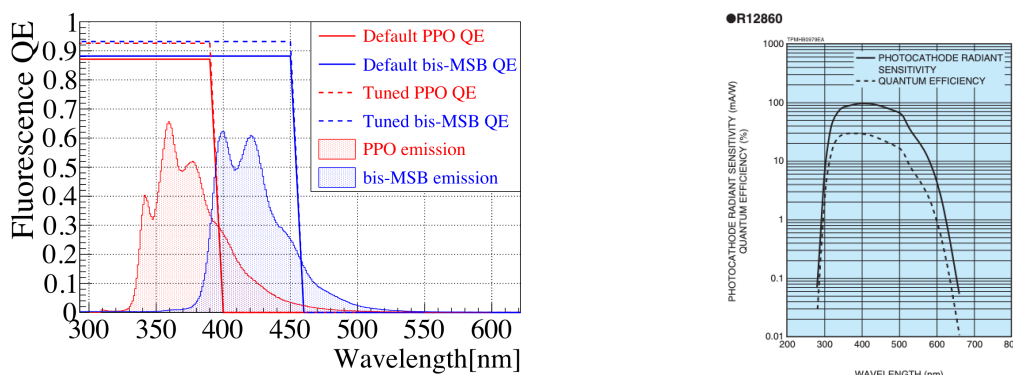


FIGURE 2.8 – On the left: Quantum efficiency (QE) and emission spectrum of the LAB and the bis-MSB [19]. On the right: Sensitivity of the Hamamatsu LPMT depending on the wavelength of the incident photons [21].

245 This formula has been optimized using dedicated studies with a Daya Bay detector [19, 22] to
246 reach the requirements for the JUNO experiment:

- 247 — A light yield / MeV of the amount of 10^4 photons to maximize the statistic in the energy
248 measurement.

- 249 — An attenuation length comparable to the size of the detector to prevent losing photons during
 250 their propagation in the LS. The final attenuation length is 25.8m [23] to compare with JUNO
 251 diameter of 35.4m.
 252 — Uranium/Thorium radiopurity to prevent background signal. The reactor neutrino program
 253 require a contamination fraction $F < 10^{-15}$ while the solar neutrino program require $F <$
 254 10^{-17} .

255 The LS will be purified before filling to reach the radiopurity and transparency requirements.
 256 The LS will frequently be purified and tested in the Online Scintillator Internal Radioactivity In-
 257 vestigation System (OSIRIS) [24] to ensure that the requirements are kept during the lifetime of the
 258 experiment.

259 Large Photo-Multipliers Tubes(LPMTs)

260 The scintillation light produced by the LS is then collected by Photo-Multipliers Tubes (PMT) that
 261 transform the incoming photon into an electric signal. As described in figure 2.9, the incident photons
 262 interact with the photocathode via photoelectric effect producing an electron called a Photo-Electron
 263 (PE). This PE is then focused on the dynodes where the high voltage will allow it to be multiplied.
 264 After multiple amplification, the electrons are read by the anode producing an electric signal that
 265 will need to be digitized by the readout electronics.

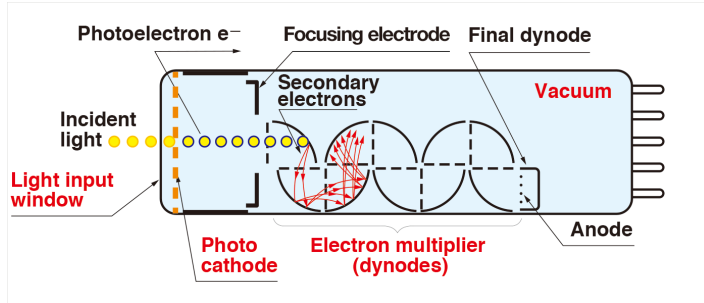


FIGURE 2.9 – Schematic of a PMT

266 The Large Photo-Multipliers Tubes (LPMT), used in the central detector and in the water pool,
 267 are 20-inch (50.8 cm) radius PMTs. ~ 5000 dynode-PMTs [21] were produced by the Hamamatsu[®]
 268 company and ~ 15000 Micro-Channel Plate (MCP) [25] by the NNVT[®] company. This system is
 269 the one responsible for the energy measurement with a energy resolution of $3\%/\sqrt{E}$, resolution
 270 necessary for the mass ordering measurement. To reach this precision, the system is composed of
 271 17612 PMTs quasi uniformly distributed over the detector for a coverage of 75.2% reaching ~ 1800
 272 PE/MeV or $\sim 2.3\%$ resolution due to statistic, leaving $\sim 0.7\%$ for the systematic uncertainties. To
 273 maintain the resolution over the lifetime of the experiment, JUNO require a failure rate $< 1\%$ over 6
 274 years.

275 The LPMTs electronic are divided in two parts. One "near", located underwater, in proximity of
 276 the LPMT to reduce the cable length between the PMT and early electronic. A second one, outside of
 277 the detector that will do higher level analysis before sending the data to the DAQ.

278 The large PE rate induce that a LPMT can collect between 1 and 1000 PE per event, causing non
 279 linearity in the PMT response that need to be understood and calibrated.

280 Small Photo-Multipliers Tubes (SPMTs)

281 The Small PMT (SPMTs), on the other hand, are 3-inch (7.62 cm) PMTs. They will be used in the
 282 CD as a secondary detection system. Those 25600 SPMTs will observe the same events as the LPMTs,
 283 thus sharing the physics and detector systematics up until the photon conversion. With a detector
 284 coverage of 2.7%, this system will collect ~ 43 PE/MeV for a final energy resolution of $\sim 17\%$.

This resolution is not enough to measure the MO, θ_{13} , Δm_{31}^2 but will be sufficient to independently measure θ_{12} and Δm_{21}^2 .

Due to the low PE rate, SPMTs will be running in photo-counting mode in the reactor range thus will be insensitive to non-linearity effect. Also, due to their smaller size and electronics, SPMTs have a better timing resolutions than the LPMTs. At higher energy range, like supernovae events, LPMTs will saturate where SPMTs due to their lower PE collection will be able to give measurement of the energy spectrum.

The Data Acquisition System (DAQ) is designed to support the event rate of IBD, background, dark noise and supplementary storage buffers are present in the LPMT electronics to withstand the event rate during supernovae burst.

2.2.3 Veto detector

The CD will be bathed in constant background noise coming from numerous, the radioactivity from surrounding rock, the radioactivity of its own components or from the cosmic muons. This background needs to be rejected to ensure the purity of the IBD spectrum. To prevent a big part of them, JUNO use two veto detector that will tag events as background before CD analysis.

Cherenkov in water pool

The Water Cherenkov Detector (WCD) is the instrumentalization of the water buffer around the CD. When high speed charged particles will pass through the water, they will produce cherenkov photons. The light will be collected by 2400 MCP LPMTs installed on the outer surface of the CD structure. The muons veto strategy is based on a PMT multiplicity condition. WCD PMTs are grouped in ten zones: 5 in the top, 5 in the bottom. Veto are raised either when more than 19 PMTs are triggered in one zone or when two adjacent zones simultaneously trigger more than 13 PMTs. Using this trigger, we expect to reach a muon detection efficiency of 99.5% while keeping the noise at reasonable level.

Top tracker

The JUNO Top Tracker (TT) is a plastic scintillator detector located on the top of the experiment (see figure 2.10). Made from plastic scintillator from OPERA [26] layered horizontally in 3 layers on the top of the detector, the TT will be able to detect incoming atmospheric muons. With its coverage, about 1/3 of the of all atmospheric muons that passing through the CD will also pass through the 3 layer of the detector. While it does not cover the majority of the detector, the TT is particularly effective to detect muons coming through the filling chimney region which might present difficulties from the other subsystems in some classes of events.

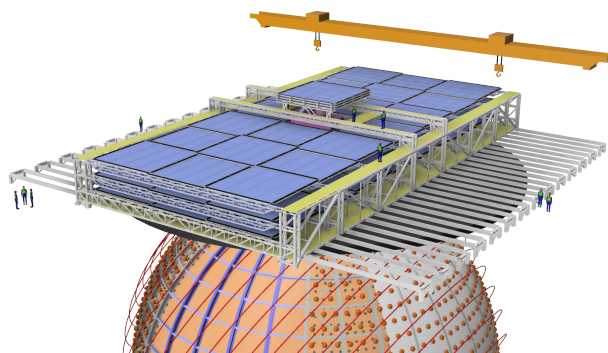


FIGURE 2.10 – The JUNO top tracker

317 2.3 Calibration strategy

318 The calibration is a crucial part of the JUNO experiment. Because we are looking at civil reactor
 319 neutrino it might be impossible to run measurement without signal, it would need to shut down
 320 every reactor from the Taishan and Yangjiang power plants which is realistically impossible. Because
 321 of this continuous rate, low frequency signal event, we need high frequency, recognisable sources in
 322 the energy range of interest, [0-12] MeV for the positron signal and 2.2 MeV for the neutron capture.
 323 It is understood that the CD response will be different depending on the type of particle and on the
 324 position on the event due to the absorption length of the LS and the optical response of the acrylic
 325 sphere (see section 2.5). The energy response is also expected to be non-linear due to the LS response
 326 [19] but also due to the saturation of the LPMTs system when collecting a large amount of PE [27].

327 2.3.1 Energy scale calibration

328 While electrons and positrons sources would be ideal, for a large LS detector, thin-walled elec-
 329 trons or positrons sources could lead to leakage of radionuclides causing contamination. Instead are
 330 considered gamma sources in the range of the prompt energy of IBDs. The sources are reported in
 331 table 2.3.

Sources / Processes	Type	Radiation
^{137}Cs	γ	0.0662 MeV
^{54}Mn	γ	0.835 MeV
^{60}Co	γ	1.173 + 1.333 MeV
^{40}K	γ	1.461 MeV
^{68}Ge	e^+	annihilation 0.511 + 0.511 MeV
$^{241}\text{Am-Be}$	n, γ	neutron + 4.43 MeV ($^{12}\text{C}^*$)
$^{241}\text{Am-}^{13}\text{C}$	n, γ	neutron + 6.13 MeV ($^{16}\text{O}^*$)
$(n, \gamma)p$	γ	2.22 MeV
$(n, \gamma)^{12}\text{C}$	γ	4.94 MeV or 3.68 + 1.26 MeV

TABLE 2.3 – List of sources and their process considered for the energy scale calibration

332 For the ^{68}Ge source, it'll decay in ^{68}Ga via electron capture, which will itself β^+ decay into ^{68}Zn .
 333 The positrons will be absorbed by the enclosure so only the annihilation gamma will be released. In
 334 addition, (α, n) sources like $^{241}\text{Am-Be}$ and $^{241}\text{Am-}^{13}\text{C}$ are used to provide both high energy gamma
 335 and neutrons, which will later be captured in the LS producing the 2.2 MeV gamma.

336 From this calibration we call E_{vis} the "visible energy" that is reconstructed by our current algo-
 337 rithms and we compare it to the true energy deposited by the calibration source. The results shown
 338 in figure 2.11 show the expected response of the detector from calibration sources. The non-linearity
 339 is clearly visible from the E_{vis}/E_{true} shape. See [28] for more details.

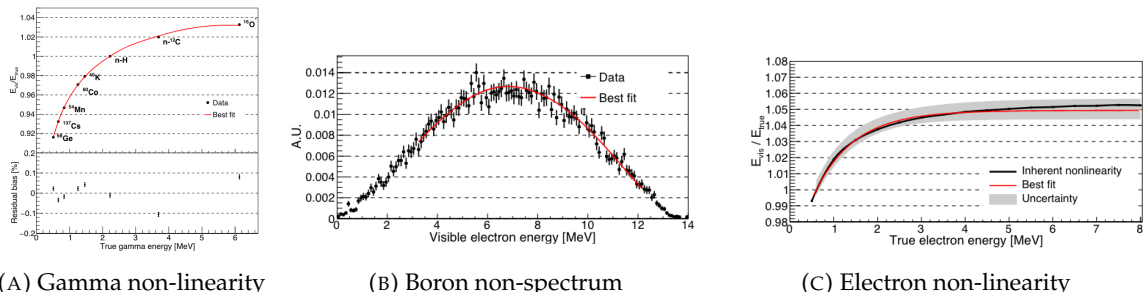


FIGURE 2.11 – Fitted and simulated non linearity of gamma and electron sources and
 ^{12}B spectrum. Black points are simulated data while red points are the best fit

340 **2.3.2 Calibration system**

341 The JUNO detector will need to investigate the non-uniformity in the detector response, more
 342 explication can be found in section 2.5. For this we can deploy sources using multiples systems that
 343 are schematized in figure 2.12 :

- 344 — For a one-dimension vertical calculation, the Automatic Calibration Unit (ACU) will be able
 345 to deploy multiple radioactive sources or a pulse laser diffuser ball along the central axis of
 346 the CD through the top chimney. The source position precision is less than 1cm.
- 347 — For off-axis calibration, a calibration source attached to a Cable Loop System (CLS) can be
 348 moved on a vertical half-plane by adjusting the length of two connection cable. Two set of
 349 CSL will be deployed to provide a 79% effective coverage of a vertical plane.
- 350 — A Guiding Tube (GT) will surround the CD to calibrate the non-uniformity of the response at
 351 the edge of the detector
- 352 — A Remotely Operated under-LS Vehicle (ROV) can be deployed to desired location inside LS
 353 for a more precise and comprehensive calibration. The ROV will also be equipped with a
 354 camera for inspection of the CD.

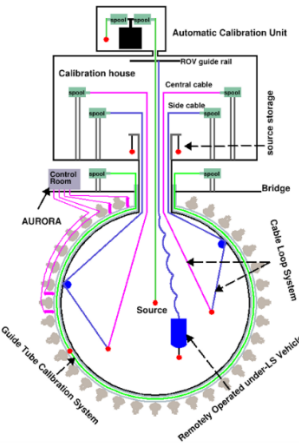


FIGURE 2.12 – Overview of the calibration system

355 The preliminary calibration program is depicted in table 2.4.

Program	Purpose	System	Duration [min]
Weekly calibration	Neutron (Am-C)	ACU	63
	Laser	ACU	78
Monthly calibration	Neutron (Am-C)	ACU	120
	Laser	ACU	147
	Neutron (Am-C)	CLS	333
	Neutron (Am-C)	GT	73
Comprehensive calibration	Neutron (Am-C)	ACU, CLS and GT	1942
	Neutron (Am-Be)	ACU	75
	Laser	ACU	391
	^{68}Ge	ACU	75
	^{137}Cs	ACU	75
	^{54}Mn	ACU	75
	^{60}Co	ACU	75
	^{40}K	ACU	158

TABLE 2.4 – Calibration program of the JUNO experiment

2.4 Software

The simulation, reconstruction and analysis algorithms are all packaged in the JUNO software, subsequently called the software. It is composed of multiple components integrated in the SNiPER [29] framework:

- Various primary particles simulators for the different kind of events, background and calibration sources.
- A Geant4 [30–32] simulation simulating the detectors geometries, a custom optical model for the LS and the supporting structures of the detectors. The Geant4 simulation integrate all relevant physics process for JUNO, validated by the collaboration. This step of the simulation is commonly called *Detsim* and compute up to the production of photo-electrons in the PMTs. The optics properties of the different materials and detector components have been measured beforehand to be used to define the material and surfaces in the simulation
- An electronic simulation, simulating the response waveform of the PMTs, tracking it through the digitization process, accounting for effects such as non-linearity, dark noise, Time Transit Spread (TTS), pre-pulsing, after-pulsing and ringing if the waveform. This step is commonly referenced as *Elecsim*.
- A waveform reconstruction where the digitized waveform are filtered to remove high-frequency white noise and then deconvoluted to yield time and charge informations of the photons hits on the PMTs. This step is commonly referenced as *Calib*.
- The charge and time informations are used by reconstruction algorithms to reconstruct the interaction vertex and the deposited energy. See section 2.5 for more details on the reconstruction.
- Once the singular events are reconstructed, they go through event pairing and classification to select IBD events.

2.5 State of the art of the IBD reconstruction in JUNO

The main reconstruction method currently run in JUNO is a data-driven method based on a likelihood maximization [33, 34]. The first step is to reconstruct the interaction vertex from which the energy reconstruction is dependent. It is also necessary for event pairing and classification.

2.5.1 Interaction vertex reconstruction

To start the likelihood maximization, a rough estimation of the vertex is made using a charge-based algorithm and a time based algorithm.

Charge based algorithm

The charge-based algorithm is basically base on the charge-weighted average of the PMT position.

$$\vec{r}_{cb} = a \cdot \text{math}$$

³⁸⁹ **2.5.2 Energy reconstruction**

³⁹⁰ **2.5.3 Particle identification**

³⁹¹ **2.5.4 Machine learning for reconstruction**

³⁹² **Vertex reconstruction**

³⁹³ **Energy reconstruction**

³⁹⁴ **2.6 JUNO sensitivity to NMO and precise measurements**

³⁹⁵ **2.6.1 Fitting procedure**

³⁹⁶ **Chapter 3**

³⁹⁷ **Machine learning and Artificial
³⁹⁸ Neural Network**

³⁹⁹ **3.1 History of the Machine learning**

⁴⁰⁰ **3.2 Boosted Decision Tree (BDT)**

⁴⁰¹ **3.3 Artificial Neural Network (NN)**

⁴⁰² **3.3.1 Fully Connected Deep Neural Network (FCDNN)**

⁴⁰³ **3.3.2 Convolutional Neural Network (CNN)**

⁴⁰⁴ **3.3.3 Graph Neural Network (GNN)**

⁴⁰⁵ **3.3.4 Adversarial Neural Network (ANN)**

⁴⁰⁶ **Generative Adversarial Network (GAN)**

⁴⁰⁷ **Reinforcement Learning (RL)**

⁴⁰⁸ **Random Search (RS)**

⁴⁰⁹ **Bayesian Optimization**

⁴¹⁰ **Chapter 4**

⁴¹¹ **Image recognition for IBD
reconstruction with the SPMT system**

⁴¹²

⁴¹³ **Chapter 5**

⁴¹⁴ **Graph representation of JUNO for IBD
reconstruction with the LPMT system**

⁴¹⁵

⁴¹⁶ Chapter 6

⁴¹⁷ **Reliability of machine learning
methods**

⁴¹⁸

⁴¹⁹ **Chapter 7**

⁴²⁰ **Discrimination of e+/e- events in
JUNO**

⁴²¹

⁴²² **Chapter 8**

⁴²³ **Conclusion**

Bibliography

- [1] Liang Zhan, Yifang Wang, Jun Cao, and Liangjian Wen. "Determination of the Neutrino Mass Hierarchy at an Intermediate Baseline". *Physical Review D* 78.11 (Dec. 10, 2008), 111103. ISSN: 1550-7998, 1550-2368. DOI: [10.1103/PhysRevD.78.111103](https://doi.org/10.1103/PhysRevD.78.111103). eprint: [0807.3203\[hep-ex, physics:hep-ph\]](https://arxiv.org/abs/0807.3203). URL: [http://arxiv.org/abs/0807.3203](https://arxiv.org/abs/0807.3203) (visited on 09/18/2023).
- [2] Fengpeng An et al. "Neutrino Physics with JUNO". *Journal of Physics G: Nuclear and Particle Physics* 43.3 (Mar. 1, 2016), 030401. ISSN: 0954-3899, 1361-6471. DOI: [10.1088/0954-3899/43/3/030401](https://doi.org/10.1088/0954-3899/43/3/030401). eprint: [1507.05613\[hep-ex, physics:physics\]](https://arxiv.org/abs/1507.05613). URL: [http://arxiv.org/abs/1507.05613](https://arxiv.org/abs/1507.05613) (visited on 07/28/2023).
- [3] A. A. Hahn, K. Schreckenbach, W. Gelletly, F. von Feilitzsch, G. Colvin, and B. Krusche. "Antineutrino spectra from 241Pu and 239Pu thermal neutron fission products". *Physics Letters B* 218.3 (Feb. 23, 1989), 365–368. ISSN: 0370-2693. DOI: [10.1016/0370-2693\(89\)91598-0](https://doi.org/10.1016/0370-2693(89)91598-0). URL: <https://www.sciencedirect.com/science/article/pii/0370269389915980> (visited on 01/16/2024).
- [4] Th A. Mueller et al. "Improved Predictions of Reactor Antineutrino Spectra". *Physical Review C* 83.5 (May 23, 2011), 054615. ISSN: 0556-2813, 1089-490X. DOI: [10.1103/PhysRevC.83.054615](https://doi.org/10.1103/PhysRevC.83.054615). eprint: [1101.2663\[hep-ex, physics:nucl-ex\]](https://arxiv.org/abs/1101.2663). URL: [http://arxiv.org/abs/1101.2663](https://arxiv.org/abs/1101.2663) (visited on 01/16/2024).
- [5] F. von Feilitzsch, A. A. Hahn, and K. Schreckenbach. "Experimental beta-spectra from 239Pu and 235U thermal neutron fission products and their correlated antineutrino spectra". *Physics Letters B* 118.1 (Dec. 2, 1982), 162–166. ISSN: 0370-2693. DOI: [10.1016/0370-2693\(82\)90622-0](https://doi.org/10.1016/0370-2693(82)90622-0). URL: <https://www.sciencedirect.com/science/article/pii/0370269382906220> (visited on 01/16/2024).
- [6] K. Schreckenbach, G. Colvin, W. Gelletly, and F. Von Feilitzsch. "Determination of the antineutrino spectrum from 235U thermal neutron fission products up to 9.5 MeV". *Physics Letters B* 160.4 (Oct. 10, 1985), 325–330. ISSN: 0370-2693. DOI: [10.1016/0370-2693\(85\)91337-1](https://doi.org/10.1016/0370-2693(85)91337-1). URL: <https://www.sciencedirect.com/science/article/pii/0370269385913371> (visited on 01/16/2024).
- [7] Patrick Huber. "On the determination of anti-neutrino spectra from nuclear reactors". *Physical Review C* 84.2 (Aug. 29, 2011), 024617. ISSN: 0556-2813, 1089-490X. DOI: [10.1103/PhysRevC.84.024617](https://doi.org/10.1103/PhysRevC.84.024617). eprint: [1106.0687\[hep-ex, physics:hep-ph, physics:nucl-ex, physics:nucl-th\]](https://arxiv.org/abs/1106.0687). URL: [http://arxiv.org/abs/1106.0687](https://arxiv.org/abs/1106.0687) (visited on 01/16/2024).
- [8] P. Vogel, G. K. Schenter, F. M. Mann, and R. E. Schenter. "Reactor antineutrino spectra and their application to antineutrino-induced reactions. II". *Physical Review C* 24.4 (Oct. 1, 1981). Publisher: American Physical Society, 1543–1553. DOI: [10.1103/PhysRevC.24.1543](https://doi.org/10.1103/PhysRevC.24.1543). URL: <https://link.aps.org/doi/10.1103/PhysRevC.24.1543> (visited on 01/16/2024).
- [9] D. A. Dwyer and T. J. Langford. "Spectral Structure of Electron Antineutrinos from Nuclear Reactors". *Physical Review Letters* 114.1 (Jan. 7, 2015), 012502. ISSN: 0031-9007, 1079-7114. DOI: [10.1103/PhysRevLett.114.012502](https://doi.org/10.1103/PhysRevLett.114.012502). eprint: [1407.1281\[hep-ex, physics:nucl-ex\]](https://arxiv.org/abs/1407.1281). URL: [http://arxiv.org/abs/1407.1281](https://arxiv.org/abs/1407.1281) (visited on 01/16/2024).

- [10] JUNO Collaboration et al. "Sub-percent Precision Measurement of Neutrino Oscillation Parameters with JUNO". *Chinese Physics C* 46.12 (Dec. 1, 2022), 123001. ISSN: 1674-1137, 2058-6132. DOI: [10.1088/1674-1137/ac8bc9](https://doi.org/10.1088/1674-1137/ac8bc9). eprint: [2204.13249\[hep-ex\]](https://arxiv.org/abs/2204.13249). URL: <http://arxiv.org/abs/2204.13249> (visited on 08/11/2023).
- [11] JUNO Collaboration et al. *TAO Conceptual Design Report: A Precision Measurement of the Reactor Antineutrino Spectrum with Sub-percent Energy Resolution*. May 18, 2020. DOI: [10.48550/arXiv.2005.08745](https://doi.org/10.48550/arXiv.2005.08745). eprint: [2005.08745\[hep-ex, physics:nucl-ex, physics:physics\]](https://arxiv.org/abs/2005.08745). URL: <http://arxiv.org/abs/2005.08745> (visited on 01/18/2024).
- [12] G. Mention, M. Fechner, Th Lasserre, Th A. Mueller, D. Lhuillier, M. Cribier, and A. Letourneau. "The Reactor Antineutrino Anomaly". *Physical Review D* 83.7 (Apr. 29, 2011), 073006. ISSN: 1550-7998, 1550-2368. DOI: [10.1103/PhysRevD.83.073006](https://doi.org/10.1103/PhysRevD.83.073006). eprint: [1101.2755\[hep-ex, physics:hep-ph\]](https://arxiv.org/abs/1101.2755). URL: <http://arxiv.org/abs/1101.2755> (visited on 01/25/2024).
- [13] V. Kopeikin, M. Skorokhvatov, and O. Titov. "Reevaluating reactor antineutrino spectra with new measurements of the ratio between ^{235}U and ^{239}Pu β spectra". *Physical Review D* 104.7 (Oct. 25, 2021), L071301. ISSN: 2470-0010, 2470-0029. DOI: [10.1103/PhysRevD.104.L071301](https://doi.org/10.1103/PhysRevD.104.L071301). eprint: [2103.01684\[hep-ph, physics:nucl-ex, physics:nucl-th\]](https://arxiv.org/abs/2103.01684). URL: <http://arxiv.org/abs/2103.01684> (visited on 01/18/2024).
- [14] A. Letourneau et al. "On the origin of the reactor antineutrino anomalies in light of a new summation model with parameterized β^- transitions". *Physical Review Letters* 130.2 (Jan. 10, 2023), 021801. ISSN: 0031-9007, 1079-7114. DOI: [10.1103/PhysRevLett.130.021801](https://doi.org/10.1103/PhysRevLett.130.021801). eprint: [2205.14954\[hep-ex, physics:hep-ph\]](https://arxiv.org/abs/2205.14954). URL: <http://arxiv.org/abs/2205.14954> (visited on 01/16/2024).
- [15] Liang Zhan, Yifang Wang, Jun Cao, and Liangjian Wen. "Experimental Requirements to Determine the Neutrino Mass Hierarchy Using Reactor Neutrinos". *Physical Review D* 79.7 (Apr. 14, 2009), 073007. ISSN: 1550-7998, 1550-2368. DOI: [10.1103/PhysRevD.79.073007](https://doi.org/10.1103/PhysRevD.79.073007). eprint: [0901.2976\[hep-ex\]](https://arxiv.org/abs/0901.2976). URL: <http://arxiv.org/abs/0901.2976> (visited on 09/18/2023).
- [16] Particle Data Group et al. "Review of Particle Physics". *Progress of Theoretical and Experimental Physics* 2020.8 (Aug. 14, 2020), 083C01. ISSN: 2050-3911. DOI: [10.1093/ptep/ptaa104](https://doi.org/10.1093/ptep/ptaa104). URL: <https://doi.org/10.1093/ptep/ptaa104> (visited on 12/04/2023).
- [17] Super-Kamiokande Collaboration et al. "Diffuse Supernova Neutrino Background Search at Super-Kamiokande". *Physical Review D* 104.12 (Dec. 10, 2021), 122002. ISSN: 2470-0010, 2470-0029. DOI: [10.1103/PhysRevD.104.122002](https://doi.org/10.1103/PhysRevD.104.122002). eprint: [2109.11174\[astro-ph, physics:hep-ex\]](https://arxiv.org/abs/2109.11174). URL: <http://arxiv.org/abs/2109.11174> (visited on 02/28/2024).
- [18] Alessandro Strumia and Francesco Vissani. "Precise quasielastic neutrino/nucleon cross section". *Physics Letters B* 564.1 (July 2003), 42–54. ISSN: 03702693. DOI: [10.1016/S0370-2693\(03\)00616-6](https://doi.org/10.1016/S0370-2693(03)00616-6). eprint: [astro-ph/0302055](https://arxiv.org/abs/astro-ph/0302055). URL: <http://arxiv.org/abs/astro-ph/0302055> (visited on 01/16/2024).
- [19] Daya Bay et al. *Optimization of the JUNO liquid scintillator composition using a Daya Bay antineutrino detector*. July 1, 2020. DOI: [10.48550/arXiv.2007.00314](https://doi.org/10.48550/arXiv.2007.00314). eprint: [2007.00314\[hep-ex, physics:physics\]](https://arxiv.org/abs/2007.00314). URL: <http://arxiv.org/abs/2007.00314> (visited on 07/26/2023).
- [20] J. B. Birks. "CHAPTER 3 - THE SCINTILLATION PROCESS IN ORGANIC MATERIALS—I". *The Theory and Practice of Scintillation Counting*. Ed. by J. B. Birks. International Series of Monographs in Electronics and Instrumentation. Jan. 1, 1964, 39–67. ISBN: 978-0-08-010472-0. DOI: [10.1016/B978-0-08-010472-0.50008-2](https://doi.org/10.1016/B978-0-08-010472-0.50008-2). URL: <https://www.sciencedirect.com/science/article/pii/B9780080104720500082> (visited on 02/07/2024).
- [21] Photomultiplier tube R12860 | Hamamatsu Photonics. URL: https://www.hamamatsu.com/eu/en/product/optical-sensors/pmt/pmt_tube-alone/head-on-type/R12860.html (visited on 02/08/2024).

- [22] Yan Zhang, Ze-Yuan Yu, Xin-Ying Li, Zi-Yan Deng, and Liang-Jian Wen. "A complete optical model for liquid-scintillator detectors". *Nuclear Instruments and Methods in Physics Research Section A: Accelerators, Spectrometers, Detectors and Associated Equipment* 967 (July 2020), 163860. ISSN: 01689002. DOI: [10.1016/j.nima.2020.163860](https://doi.org/10.1016/j.nima.2020.163860). eprint: [2003.12212\[physics\]](https://arxiv.org/abs/2003.12212). URL: <http://arxiv.org/abs/2003.12212> (visited on 02/07/2024).
- [23] Hai-Bo Yang et al. "Light Attenuation Length of High Quality Linear Alkyl Benzene as Liquid Scintillator Solvent for the JUNO Experiment". *Journal of Instrumentation* 12.11 (Nov. 27, 2017), T11004–T11004. ISSN: 1748-0221. DOI: [10.1088/1748-0221/12/11/T11004](https://doi.org/10.1088/1748-0221/12/11/T11004). eprint: [1703.01867\[hep-ex, physics:physics\]](https://arxiv.org/abs/1703.01867). URL: <http://arxiv.org/abs/1703.01867> (visited on 07/28/2023).
- [24] JUNO Collaboration et al. *The Design and Sensitivity of JUNO's scintillator radiopurity pre-detector OSIRIS*. Mar. 31, 2021. DOI: [10.48550/arXiv.2103.16900](https://doi.org/10.48550/arXiv.2103.16900). eprint: [2103.16900\[physics\]](https://arxiv.org/abs/2103.16900). URL: <http://arxiv.org/abs/2103.16900> (visited on 02/07/2024).
- [25] Angel Abusleme et al. "Mass Testing and Characterization of 20-inch PMTs for JUNO". *The European Physical Journal C* 82.12 (Dec. 24, 2022), 1168. ISSN: 1434-6052. DOI: [10.1140/epjc/s10052-022-11002-8](https://doi.org/10.1140/epjc/s10052-022-11002-8). eprint: [2205.08629\[hep-ex, physics:physics\]](https://arxiv.org/abs/2205.08629). URL: <http://arxiv.org/abs/2205.08629> (visited on 02/08/2024).
- [26] R. Acquafredda et al. "The OPERA experiment in the CERN to Gran Sasso neutrino beam". *Journal of Instrumentation* 4.4 (Apr. 2009), P04018. ISSN: 1748-0221. DOI: [10.1088/1748-0221/4/04/P04018](https://doi.org/10.1088/1748-0221/4/04/P04018). URL: <https://dx.doi.org/10.1088/1748-0221/4/04/P04018> (visited on 02/29/2024).
- [27] Yang Han. "Dual Calorimetry for High Precision Neutrino Oscillation Measurement at JUNO Experiment". AstroParticule et Cosmologie, France, Paris U. VII, APC, Not specified, June 2021.
- [28] JUNO collaboration et al. "Calibration Strategy of the JUNO Experiment". *Journal of High Energy Physics* 2021.3 (Mar. 2021), 4. ISSN: 1029-8479. DOI: [10.1007/JHEP03\(2021\)004](https://doi.org/10.1007/JHEP03(2021)004). eprint: [2011.06405\[hep-ex, physics:physics\]](https://arxiv.org/abs/2011.06405). URL: <http://arxiv.org/abs/2011.06405> (visited on 08/10/2023).
- [29] Tao Lin et al. "The Application of SNiPER to the JUNO Simulation". *Journal of Physics: Conference Series* 898.4 (Oct. 2017). Publisher: IOP Publishing, 042029. ISSN: 1742-6596. DOI: [10.1088/1742-6596/898/4/042029](https://doi.org/10.1088/1742-6596/898/4/042029). URL: <https://dx.doi.org/10.1088/1742-6596/898/4/042029> (visited on 02/27/2024).
- [30] S. Agostinelli et al. "Geant4—a simulation toolkit". *Nuclear Instruments and Methods in Physics Research Section A: Accelerators, Spectrometers, Detectors and Associated Equipment* 506.3 (July 1, 2003), 250–303. ISSN: 0168-9002. DOI: [10.1016/S0168-9002\(03\)01368-8](https://doi.org/10.1016/S0168-9002(03)01368-8). URL: <https://www.sciencedirect.com/science/article/pii/S0168900203013688> (visited on 02/27/2024).
- [31] J. Allison et al. "Geant4 developments and applications". *IEEE Transactions on Nuclear Science* 53.1 (Feb. 2006). Conference Name: IEEE Transactions on Nuclear Science, 270–278. ISSN: 1558-1578. DOI: [10.1109/TNS.2006.869826](https://doi.org/10.1109/TNS.2006.869826). URL: <https://ieeexplore.ieee.org/document/1610988?isnumber=33833&arnumber=1610988&count=33&index=7> (visited on 02/27/2024).
- [32] J. Allison et al. "Recent developments in Geant4". *Nuclear Instruments and Methods in Physics Research Section A: Accelerators, Spectrometers, Detectors and Associated Equipment* 835 (Nov. 1, 2016), 186–225. ISSN: 0168-9002. DOI: [10.1016/j.nima.2016.06.125](https://doi.org/10.1016/j.nima.2016.06.125). URL: <https://www.sciencedirect.com/science/article/pii/S0168900216306957> (visited on 02/27/2024).
- [33] Wenjie Wu, Miao He, Xiang Zhou, and Haoxue Qiao. "A new method of energy reconstruction for large spherical liquid scintillator detectors". *Journal of Instrumentation* 14.3 (Mar. 8, 2019), P03009–P03009. ISSN: 1748-0221. DOI: [10.1088/1748-0221/14/03/P03009](https://doi.org/10.1088/1748-0221/14/03/P03009). eprint: [1812.01799\[hep-ex, physics:physics\]](https://arxiv.org/abs/1812.01799). URL: <http://arxiv.org/abs/1812.01799> (visited on 07/28/2023).

- 561 [34] Guihong Huang et al. "Improving the energy uniformity for large liquid scintillator detec-
562 tors". *Nuclear Instruments and Methods in Physics Research Section A: Accelerators, Spectrometers,*
563 *Detectors and Associated Equipment* 1001 (June 11, 2021), 165287. ISSN: 0168-9002. DOI: [10.1016/j.nima.2021.165287](https://doi.org/10.1016/j.nima.2021.165287). URL: <https://www.sciencedirect.com/science/article/pii/S0168900221002710> (visited on 03/01/2024).
- 564
565